Journal of Physics D: Applied Physics

The Epitaxial Growth and Unique Morphology of InAs Quantum Dots Embedded in a Ge Matrix

To cite this article before publication: Hui Jia *et al* 2022 *J. Phys. D: Appl. Phys.* in press https://doi.org/10.1088/1361-6463/ac95a3

IOP Publishing Journal Title
Journal **XX** (XXXX) XXXXXX https://doi.org/XXXX/XXXX

The Epitaxial Growth and Unique Morphology of InAs Quantum Dots Embedded in a Ge Matrix

Hui Jia[1], Junjie Yang[1], Mingchu Tang[1], Wei Li[2], Pamela Jurczak[1], Xuezhe Yu[1], Taojie Zhou[1], Jae-seong Park[1], Keshuang Li[1], Huiwen Deng[1], Xueying Yu[1], Ang Li[2], Siming Chen[1], Alwyn Seeds[1] and Huiyun Liu[1]

[1] Department of Electronic and Electrical Engineering, University College London, Torrington Place, London, WC1E 7JE, United Kingdom

[2] Institute of the Microstructure and Properties of Advanced Materials, Beijing University of Technology, Beijing, 100124, China

E-mail: junjie.yang.13@ucl.ac.uk; mingchu.tang.11@ucl.ac.uk; huiyun.liu@ucl.ac.uk

Received xxxxxx
Accepted for publication xxxxxx
Published xxxxxx

Abstract

In this work, we investigated the epitaxial growth of InAs quantum dots (QDs) on Ge substrates. By varying the growth parameters of growth temperature, deposition thickness and growth rate of InAs, a high density of 1.2×10^{11} cm^{-2} self-assembled InAs QDs were successfully epitaxially grown on Ge substrates by solid-source molecular beam epitaxy (MBE) and capped by Ge layers. Pyramidal- and polyhedral-shaped InAs QDs embedded in Ge matrices were revealed, which are distinct from the lens- or truncated pyramid-shape dots in InAs/GaAs or InAs/Si systems. Moreover, with 200 nm Ge capping layer, one third of the embedded QDs are found with ellipse and hexagonal nanovoids with sizes of 7 – 9 nm, which is observed for the first time for InAs QDs embedded in a Ge matrix to the best of our knowledge. These results provide a new possibility of integrating InAs QD devices on Group-IV platforms for Si photonics.

Keywords: quantum dots, germanium, molecular beam epitaxy, nanovoids

1. Introduction

The epitaxial growth of InAs QDs on GaAs substrates and GaAs/(Ge)/Si substrates has been tremendously investigated for the pursuit of optoelectronic applications such as lasers [1] and photodetectors on Si [2]. The almost identical lattice constants and thermal expansion coefficients (TEC) of Ge and GaAs make Ge a promising substitute to GaAs substrate. Ge substrates are not only advantageous in mechanical strength and crystal quality, but also are available in larger scale wafers

of 8 inch. More importantly, it is capable to integrate with Si substrate with a Ge thin buffer [3].

Until now, the heteroepitaxial growth of InAs QDs directly on Si or Ge substrates has been rarely reported by several groups where different dot morphology and density are investigated. For example, large dome-shaped InAs QDs with sizes of 30-70 nm were grown at 400 °C on a hydrogen-terminated Si (100) substrate with a density of 1.3×10^{10} cm^{-2} [4]. Later, high uniformity InAs QDs grown on Si substrates were demonstrated with dot density of ~10^{11} cm^{-2} and 1.3 μm wavelength photoluminescence emission [5, 6]. Recently, nearly strain-relaxed InAs QDs embedded in a defect-free Si matrix have been demonstrated by a combination of several steps of overgrowth and post-growth annealing processes [7]. As for the epitaxial growth of InAs QDs directly on Ge, InAs and InGaAs islands were grown on 6° offcut Ge (100) substrate by metalorganic vapour phase epitaxy. The highest island density achieved was 2.5×10^{10} cm^{-2} and photoluminescence from InAs islands was only observed when embedded in GaAs capping layers [8, 9].

Compared with InAs QDs directly embedded in Si, where the critical radius of nanoclusters is just a couple of nanometres due to the large heteroepitaxial strain of 11.6 % [10], the size tunability of InAs QD in Ge is comparatively higher[5, 9]. In addition, the highly-lattice-mismatched InAs-Si heteroepitaxial growth is easy to produce mesoscopic dislocated clusters instead of nanoscale QDs [11]. The InAs/Ge system can also be easily buried into a Si matrix to provide better carrier confinement. Inspired by the above-mentioned advantages, in this paper, we have investigated the growth mechanism of InAs QDs directly grown on Ge substrate, by varying the growth temperature, deposition thickness and growth rate of InAs, which results a high density InAs/Ge QDs of 1.2×10^{11} cm^{-2}. Furthermore, the overgrowth of Ge capping layer was examined with 40 nm and 200 nm, respectively. The QD morphology has been changed during the different capping process. By understanding the mechanism of InAs QDs grown on Ge substrate, the Ge/InAs QDs/Ge stack can potentially be a candidate for new generation Si-based optoelectronic devices in the future, of which the growth is fully CMOS compatible, low-cost, and feasible.

2. Material epitaxial growth and characterisation

The material epitaxial growth were caried out in a twin-chamber Veeco Gen-930 solid-source MBE system, where wafers can be transferred under ultra-high vacuum condition between III-V and Group-IV growth chambers, ensuring a clean epi-surface. 2-inch P$^+$ Ge (100) wafers were first degassed in the preparation chamber at 400 °C and then deoxidised at 600-700 °C in the Group-IV growth chamber. The wafers were then transferred to the III-V growth chamber for InAs QD growth. After finding the comparatively optimal growth condition, wafers were transferred back to the Group-IV chamber for Ge overgrowth. Based on the optimal QD growth conditions, different thickness of Ge overgrowth, 40 nm and 200 nm, were carried out using a two-step growth method, separately. The Ge overgrowth was started with a 20 nm-thick low temperature growth at 250°C to facilitate layer-by-layer growth and finished by the high temperature Ge growths at 500 °C to remove any point defects introduced in the low-temperature growth and achieve high crystal quality of the Ge layers. The growth rates for low-temperature and high-temperature Ge growths were 0.25 Å/s (0.18 ML/s) and 0.6 Å/s (0.42 ML/s), respectively. Surface morphology was probed by atomic force microscopy (AFM). High-angle annular dark-field (HAADF) and bright-field (BF) scanning transmission electron microscopy (STEM) imaging results were presented to depict the embedded InAs QDs and the surrounding Ge matrix. All the AFM images are measured in the central area of the grown wafer.

3. Results and discussion

1.1 Growth optimisation

To find the optimal growth conditions for InAs QDs on Ge, three series of samples were grown and summarised in Table I. Prior to the growth details, as mentioned above, the Ge wafers were all deoxidised in Group-IV MBE chamber instead of direct deoxidisation in the III-V chamber for the growth, aiming to avoid As etching of Ge surface [12]. To verify the effect of As-rich environment on Ge, one p+ Ge (100) wafer was loaded into the III-V growth chamber and heated to ~ 400 °C with an As background. As_2 molecules of a beam-equivalent pressure (BEP) of 5×10^{-6} Torr were supplied for 10 minutes. After that, the sample was taken out for surface probing. 1×1 μm^2 and 5×5 μm^2 AFM results are shown in Figure 1(a) and Figure 1(b), respectively. AFM image of Ge surface just after deoxidation without any As background is also presented as a reference, as shown in Figure 1(c), where shows no ordered surface patterns. In contrast, etched step edges can be clearly seen from Figure 1(a). Such etching happened in directions both along and perpendicular to the step edge. The height profile across the surface, as indicated by the white line in Figure 1(a), is shown in Figure 1(d), with a step height of approximately 2.36 Å, which is near to the theoretical double atomic step (2.83 Å). In a larger scale AFM images as shown in Figure 1(b), sawtooth-like surface constructions are observed, which are similar to the dendritic single steps in hydrogen annealed Si surface explained to be a result of dimer-vacancy row crossing the terraces in either [110] or [1-10] direction [13].

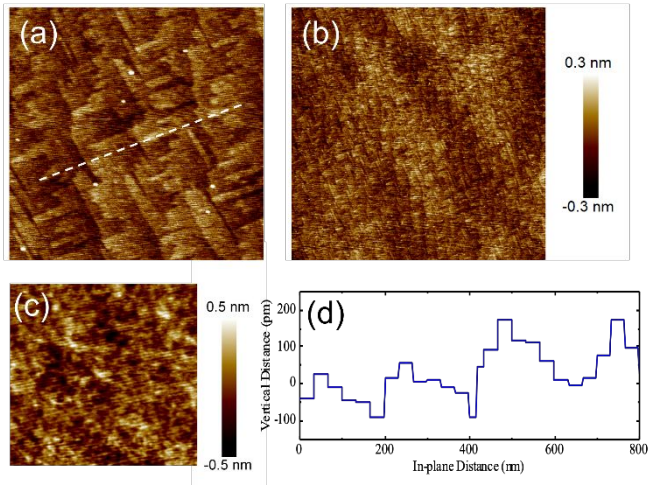

Figure 1. AFM images of central parts of background As-etched Ge surface of (a) 1 × 1 μm² and (b) 5 × 5 μm², and (c) 1 × 1 μm² AFM image of Ge substrate surface after deoxidation without any As background. (d) Surface height profile of the white dash line in (a).

Table I. Parameters of layer-by-layer deposited Ge/InAs/Ge substrate.

Sample	Substrate temperature, °C	InAs coverage, ML	Growth rate, ML/s	Cap layer	Dot density, × 10^{10} cm^{-2}
A	450	2.1	0.15	No	0.40
B	430	2.1	0.15	No	0.43
C	410	2.1	0.15	No	1.38
D	390	2.1	0.15	No	1.65
E	360	2.1	0.15	No	2.21
F	360	1.8	0.15	No	6.18
G	360	1.65	0.15	No	0.37
H	360	1.49	0.135	No	2.88
I	360	1.32	0.12	No	11.6
J	360	1.32	0.12	40 nm	-
K	360	1.32	0.12	200 nm	-

After the deoxidation, wafers were directly transferred to the III-V growth chamber for QD growth. The growth was initiated based on our optimised growth techniques for III-V on Ge by applying a Group-III pre-layer [14]. For each sample, 1 ML In was deposited on Ge first without As flux at the same temperature and growth rate as QD growth. Then As_2 overpressure was provided for 10 seconds to fully passivate the In monolayer. Although the In BEP varied with different In growth rates, a fixed V/III ratio of 55 was used for QD growth. For example, for QD growth with an In growth rate of 0.15 ML/s, the BEP of In was 9 × 10^{-8} Torr and that of As_2 was 5 × 10^{-6} Torr. Three series of samples were grown to investigate the effects of substrate temperature, InAs coverage and growth rate on the dot morphology and density. In the first series (samples A – E), an In pre-layer, an InAs coverage of 2.1 ML and a growth rate of 0.15 ML/s were used as a starting point to find the optimal growth temperature. Figure 2(a) – (e) shows 1 × 1 μm² AFM images of samples A – E, respectively.

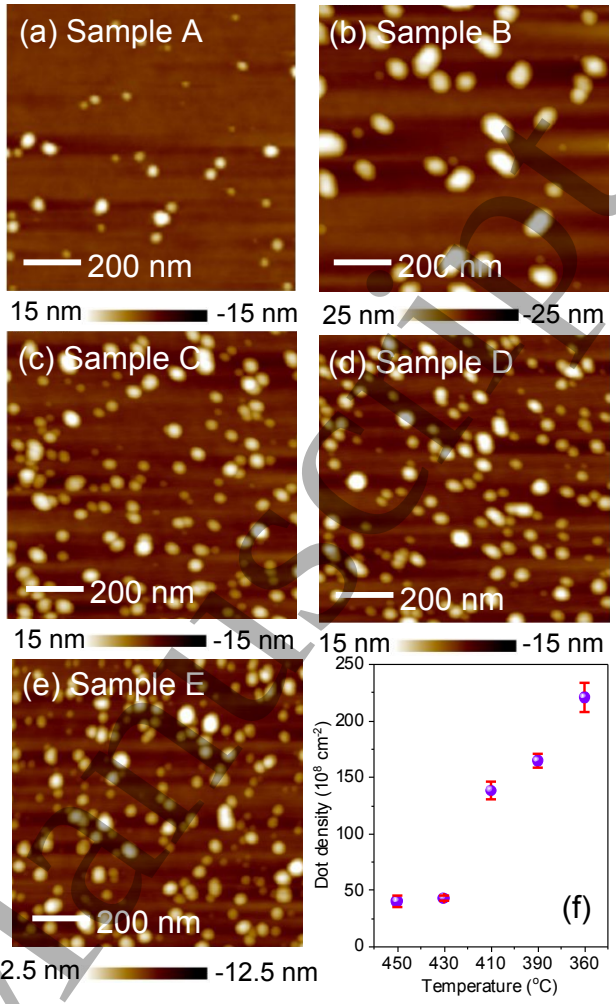

Figure 2. 1 × 1 μm² AFM images of the central parts of samples grown at (a) 450 °C, (b) 430 °C, (c) 410 °C, (d) 390 °C, and (e) 360 °C. (f) is the dot density change with growth temperature.

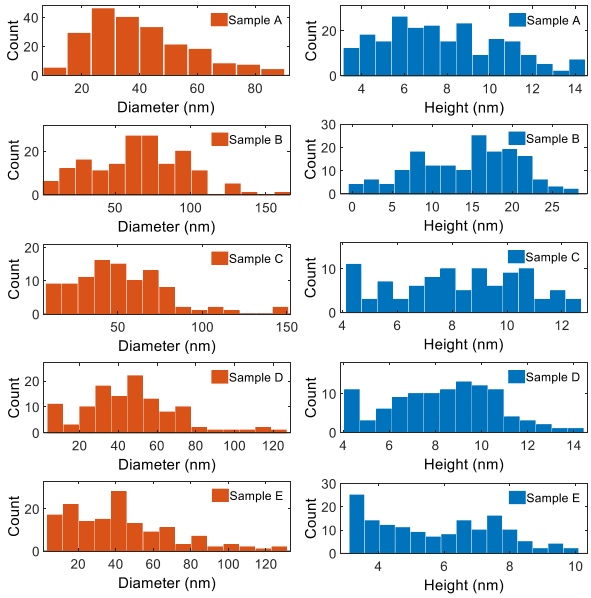

Figure 3. Dot diameter and height histograms of samples A – E.

The dot diameter and height histograms of samples A – E are presented in Figure 3. A clear trend of increasing dot density with decreasing substrate temperature was found (from samples B – E). The dot density is increased from (4.28 ± 0.38) × 10^9 cm^{-2} (sample B) to (2.21 ± 0.13) × 10^{10} cm^{-2} (sample E), as shown in Figure 2(f). For samples A and B the dot densities are almost the same, which are (4.0 ± 0.44) × 10^9 cm^{-2} and (4.3 ± 0.38) × 10^9 cm^{-2}, respectively. Normally, the dot density should increase with decreasing growth temperature because of suppressed InAs desorption and increased sticking coefficient. This anomalous behaviour could be attributed to the coalescence of the adjacent dots [9] and/or a coarsening dynamics of Ostwald ripening, due to material exchanges between the growing QDs, which is favoured at high mobility. Further decrease in growth temperature showed no significant positive effect on dot density, indicating that around 360 °C is the optimal temperature for InAs QD/Ge growth. A typical size of QD from samples A – E (except sample B) is with a diameter of 35 – 60 nm and a height of 4 – 12 nm.

Later, to examine the effect of InAs coverage on QD density, samples F and G were grown with decreased InAs coverages of 1.8 ML and 1.65 ML, respectively, by shortening the deposition duration while maintaining other growth parameters. The AFM image of sample F is shown in Figure 4(a). Compared with sample E, a significant improvement of the dot density is identified. However, although sample F has reached a high dot density, large amount of defect dots are also observed. This also can be seen from the diameter histogram of sample F in Figure 5, a long tail up to 60 nm is presented. Those defect dots are several times larger in dimension than others and may contain lots of crystal defects deteriorating the optical properties of the QDs. A possible formation mechanism of those defect dots is the coalescence of the adjacent dots.

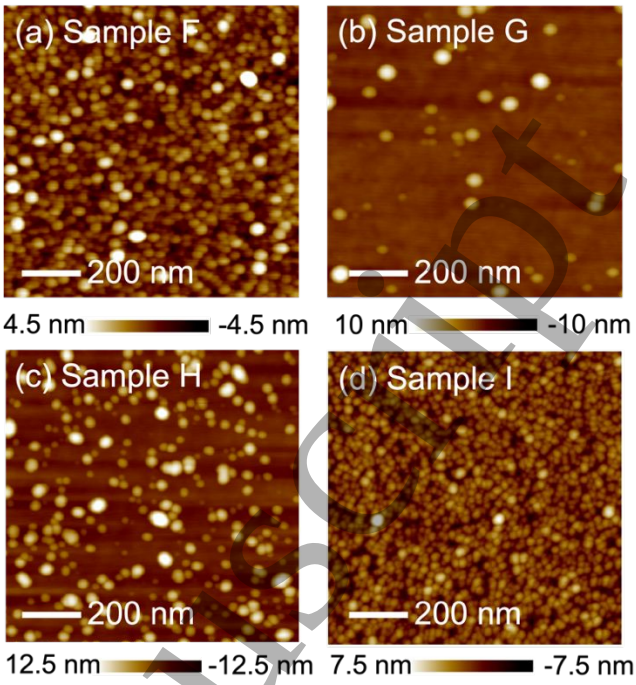

Figure 4. (a) – (d) are 1 × 1 μm² AFM images of central parts of samples F, G, H, and I, respectively.

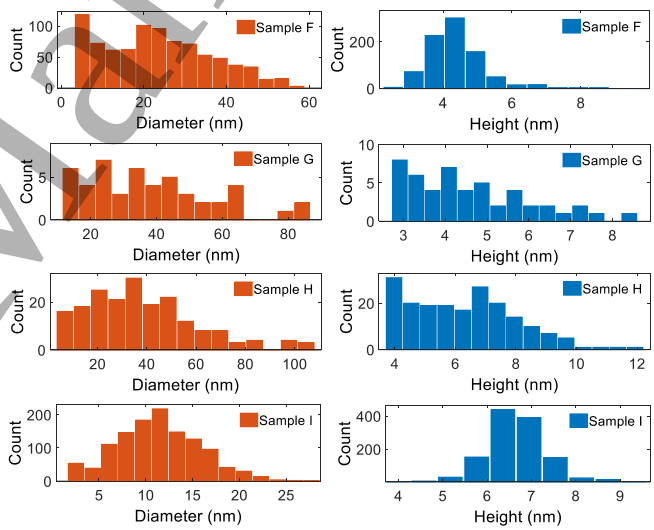

Figure 5. Dot diameter and height histograms of samples F – I. Gaussian distribution can be found for the diameter histogram of sample I and the height histograms of samples F and I.

By further decreasing the InAs coverage to 1.65 ML, the dot density in the central area of sample G, as shown in Figure 4(b), drops dramatically to 3.7 × 10^9 cm^{-2}. Indeed, as the dot density varies substantially, which is not as expected, larger scale AFM scans were performed to check the general morphology. It was found that the surface shows large undulations of heights around 30 nm decorated with clustered QDs, therefore giving rise to the large discrepancy of the surface dot density. The possible reason could be the accident surface contaminations acting as the nucleation centres for the

large undulations [15], but it needs to be investigated further in the future work. Nevertheless, from the comparison of sample E and F, beneficial impact of reducing the InAs coverage can be inferred, as the dot density has been significantly increased. Consequently, in the third group (samples H and I), the growth rates were varied from 0.135 ML/s to 0.12 ML/s, with the deposition time of 11s and the substrate temperature of 360 °C. A high QD density of 1.2×10^{11} cm^{-2} with dramatically reduced number of defect dots was achieved in sample I, as demonstrated from Figure 4 (d). The diameter and height histograms of samples F – I are shown in Figure 5. Wide diameter distribution has also been found for samples F, G and H. The height histogram improves dramatically for sample F, where Gaussian distribution centred at 4.3 nm can be seen. For sample I, both diameter and height demonstrate Gaussian distribution, and centred at 10.2 nm and 6.5 nm, respectively. A typical QD size of sample I is 5 – 18 nm in diameter and 5 – 8 nm in height. These results lead us to draw the conclusion that the growth dynamics of the QDs is a result of the coordinative changes of the growth temperature, material coverage and dot growth rate rather than the monotonic change of one variable.

3.2 Ge overgrowth

Based on the optimal growth conditions for QDs (sample I), 40 nm (sample J) and 200 nm (sample K) Ge capping layers were grown in group – IV MBE chamber using a two-step growth method. Schematic illustration of the grown structure is shown in Figure 6(a). 1×1 μm^2 and 5×5 μm^2 AFM images of the samples are shown in Figure 6(b) and (c) (sample J), and Figure 6(d) and (e) (for sample K). A smooth epi-surface with atomic steps could be clearly seen for both samples, indicating QDs have been fully covered by Ge layer, which is different from Si/InAs/Si where numerous nanoholes as large as QDs were depicted after Si overgrowth [7]. However, surface TDs with a density of $3 – 5 \times 10^8$ cm^{-2} were estimated for both 40 nm and 200 nm Ge samples, by counting the dark holes in the AFM images. Those TDs are mainly originated from misfit dislocations at the InAs/Ge interface and later travel to the surface. It is also noteworthy that the defect morphology for the thin and thick capping layer samples is different. In addition to surface TDs as observed in sample J with 40 nm Ge capping layer (see Figure 6 (b) and (c)), short-line indentation defects with similar lengths were also found in sample K with 200 nm Ge capping, as shown in Figure 6(d) and (e). The line indentation defects may be related to stacking faults (SFs) extending to the surface [16]. To find out the potential explanation for the different surface morphology of the overgrowth samples and to have a closer investigation of the novel material system, STEM measurements were applied.

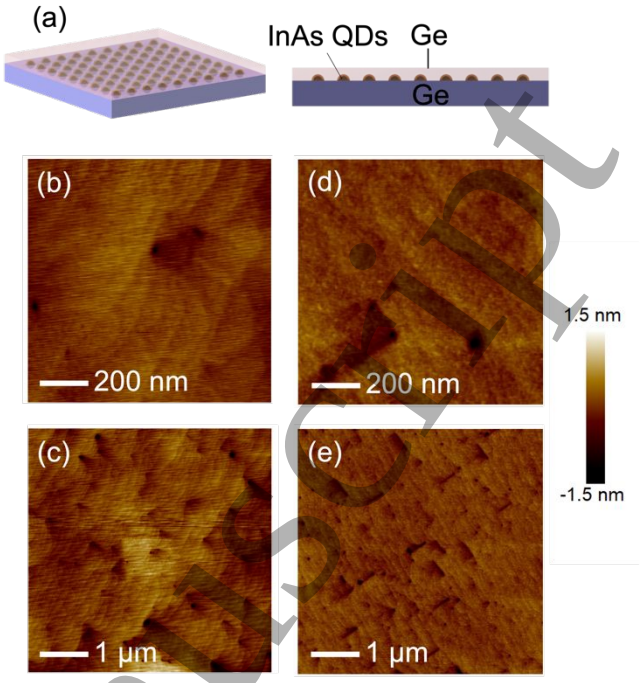

Figure 6. (a) Schematic diagram of InAs QDs embedded in a Ge matrix. (b) and (c) are 1×1 μm^2 and 5×5 μm^2 AFM images of the central parts of the QD sample covered with 40 nm Ge (sample J). (d) and (e) are those of 200 nm overgrown Ge surface (sample K).

4. STEM analysis

To investigate the morphology of the embedded InAs QD structures, large-scale STEM was first conducted. Figure 7(a) and (b) show HAADF and BF-STEM images of InAs QDs with 40 nm-thick Ge capping layers, respectively. The well-defined pyramid- and polyhedral-shaped InAs QDs with brighter colour than the Ge were observed in Figure 7(a). Continuous wetting layer and defect-free Ge matrix were also confirmed. In contrast, the InAs QD with a 200 nm-thick Ge capping layer presents clear differences in terms of the buried dot morphology and the surrounding Ge matrix, as shown in Figure 7(c) and (d). In figure 7(c), approximately one third of QDs are found with a considerably-reduced-HAADF-intensity nanostructure on the top or top corner, indicating the existence of nanovoids. Indeed, {111} defects of similar and even larger (of a shape of reversed-truncated cone) dimensions are ubiquitous in the 200 nm capped sample, ascribed to the latter capping process. The size of the above-mentioned reversed-truncated cone shape defect is consistent with the surface indentation defect shown in the AFM images (Figure 6(d) and (e)). Noted that numerous tiny spots observed in the Ge matrix for both samples are caused by sample cleavage and thus should be exempt from the structural analysis.

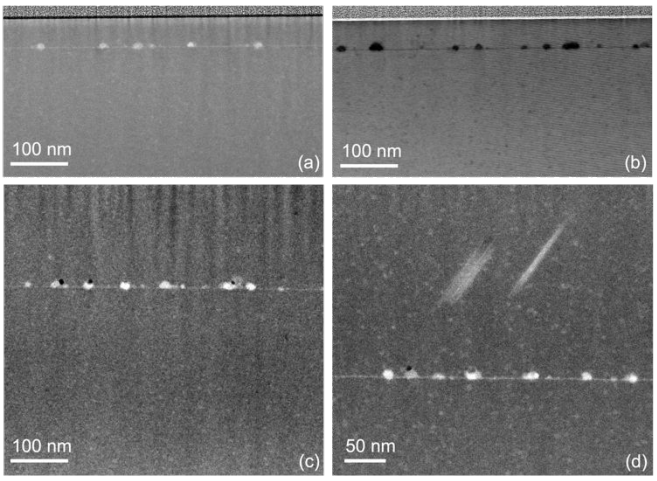

Figure 7. STEM images of InAs/Ge samples with a 40 nm (sample J) and a 200 nm (sample K) Ge capping layer. (a) and (b) are HAADF and BF images of sample J, respectively. (c) and (d) are HAADF images of sample K with different scale.

Figure 8(a) – (c) show high magnification HAADF-STEM images of selected typical QD structures in the 40 nm Ge capping layer of sample J. Several features of these QDs can be summarised from the images as below. (1) QDs have good profile showing no Ge-InAs inter-diffusion. (2) Although most of the QDs contain crystal defects, visually, none of them has propagated to the above Ge matrix. (3) The aspect ratio of the QDs is apparently smaller than that of InAs QDs grown on GaAs [17-20]. Truncated pyramid shape has been reported for InAs QDs embedded in a GaAs surrounding [20]. In our case, dots either remain a pyramid shape (Figure 8(a) dot on the right and Figure 8(b) – (c)) or has a spherical shape (Figure 8(a) dot on the left). The smaller dot of 6.2 nm in diameter and 5.8 nm in height and the larger dot of 24 nm in diameter and 11.4 nm in height are found as shown in Figure 8(a). The observed sizes of the QDs are comparable to the uncapped QDs (sample I) depicted by the AFM results in section 3.1, which means that the strain of the embedded QDs is well relaxed. The observed crystal defects of SFs, twin boundaries (TBs), or misfit dislocation loops, are marked by white dashed lines, orange solid lines and small white triangles, respectively, in Figure 8(c).

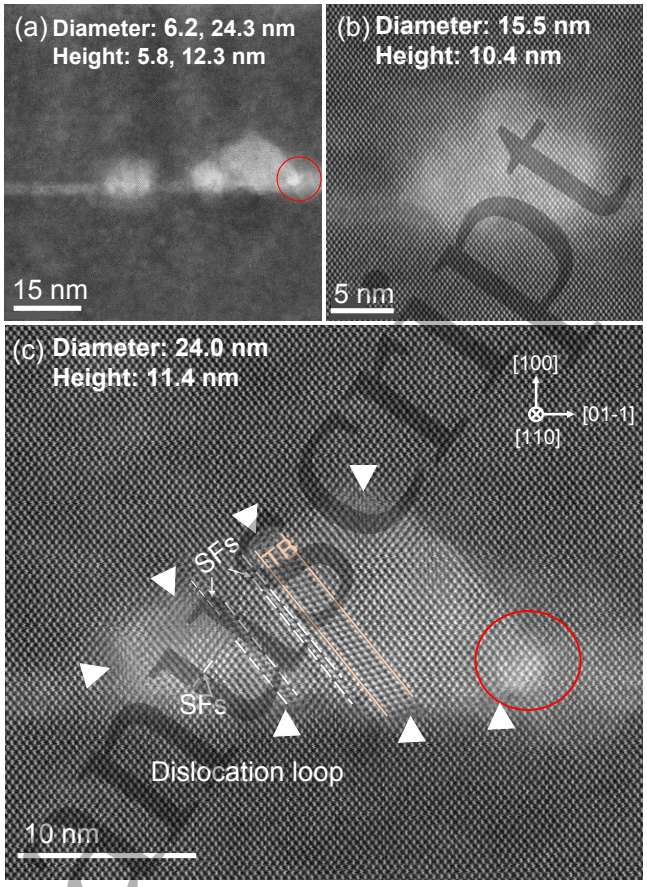

Figure 8. (a)-(c) High magnification HAADF-STEM images of sample J (QDs with 40 nm Ge cap). (a) shows different size QDs with continuous wetting layer (b) presents a typical QD with a diameter of 15.5 nm and a height of 10.4 nm with no observable crystal defects (c) demonstrates an enlarged image of a large QD with multiple crystal defects presented within the dots. Misfit dislocation loops are labelled as white triangles surrounding the QD, SFs are marked as white dash lines and twin boundaries are shown as orange solid lines. In enrichment is circled in red colour.

It is also noteworthy that the morphology discrepancy between the surface dots and buried dots may point to the important role of TEC of the dot material and the surrounding matrix. In the InAs/Si system, surface dots are mostly lens-shaped, whereas the buried dots are more spherical [7]. This is because dots are almost unstrained at the growth temperature and only strained again during after-growth cooling due to the difference in linear TEC [7]. In contrast, InAs and Ge have similar TEC, inferring less discrepancy between the morphology of surface and buried dots, which is in good agreement with that observed for sample I (uncapped dots) and J (capped dots). In addition, the wetting layer is continuous without defect even though some Ge-InAs interdiffusion is recognised, which can be seen through the darker intensity inside the wetting layers in Figure 8. This behaviour is distinct from the InAs QD on Si where

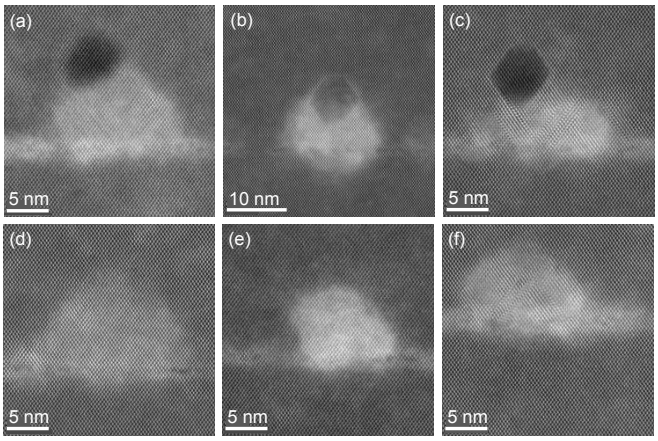

Figure 9. (a)-(f) High magnification HAADF-STEM images of 200 nm Ge capping layer sample K.

discontinuous wetting layer was reported [7]. Besides, In enrichment is detected in some dots in the basal corner of the dots, as shown in Figure 8(a) and (c) marked by red circles, and in the basal centre (figure not shown here). This behaviour is also dissimilar with that in a GaAs matrix where reversed truncated pyramid shape In enrichment is found. Last, defects are observed both in smaller and in larger dots, while dot without any defect is only found for smaller dots (~15.5 nm in diameter and 10.4 nm in height, e. g. shown in Figure 8(b)). The significantly reduced defect propagation can be explained by the formation of dislocation half-loops. They are reported to nucleate from 60° dislocations at a critical thickness, then elongate along {1,1,1} plane forming half-loops and keep expanding the diameter with the help of strain field within the material [21]. Normally these dislocation half-loops will ultimately reach the material interface and either become linear misfit segments or travel upwards as threading dislocations. In our case, the dislocation loops seem mostly form misfit segments at the InAs/Ge interface. However, there is a possibility that the threading dislocations still originate from the buried dots because of the existence of the threading segments.

The structures of the embedded QDs under 200 nm Ge cap are even more unique. First, the most unusual observation is the formation of the nanovoids, as presented in Figure 9(a) – (c). Only one third of nanovoids are of an ellipse cross section (Figure 9(a)), and the rest have a hexagonal shape with (100) facets forming the upper bound of the void and the interface with the QD, as can be seen in Figure 9(b) and (c). Both the pyramidal dots and the hexagonal voids facets have a ~ 55° angle with (100) crystal plane, which correspond to {1,1,1} facets. The hexagonal nanovoids have sharp interface with the Ge matrix, in which the facets facing each other are parallel and the two facets on each side form an obtuse of approximately ~ 108°, rendering one to link the formation of the nanovoids to the possible defect- or strain-related movement of the crystalline plane during the capping process. Besides, another important observation is that the chance to find a 'perfect' dot, i.e., without any defect, is increased for the 200 nm Ge cap sample compared with the 40 nm Ge cap sample. Two such examples are shown in Figure 9(d) and (e), where large (21.6 nm) and small (12.5 nm) dots are chosen. For QDs with a nanovoid on the top, the dot itself (which means the dot material, except the void defect) tends to be defect-free, as shown in Figure 9 (a) and (b). Nonetheless, stacking faults and misfit dislocations can occasionally be seen in dots with or without a nanovoid, as presented in Figure 9(c) and (f), respectively.

Although the formation mechanism of the nanovoid is unclear yet, two possible explanations are proposed as follows. First, the voids are caused by the In segregation during the high temperature Ge overgrowth. As mentioned in Section 3.2, the Ge overgrowth was performed by the two-temperature step method, of which the high temperature used was 500 °C and the growth duration was 50 minutes for sample K. Kept at this high temperature for a long time, the embedded QDs may experience structural changes consequently. Likewise, materials missing from QDs were also reported by Lenz et al., where after the deposition of InGaAs QDs onto GaAs substrate, about 5 nm GaAs was overgrown at 500 °C followed by a 600 seconds long interruption at elevated temperature of 600 °C [22]. From their observations, small dots were not affected, while larger and thus more strained dots first were truncated and then suffered from severe In eruption, which was confirmed from the occurrence of sub-monolayer In, and afterwards are unable to be fully filled due to the formation of either concave top facet or void within the QD [22]. Moreover, hexagonal-shaped void has also been documented in metalorganic chemical vapour deposition of N-polar AlN film on sapphire substrate, where the oxygen out-diffusion was accused of the formation of the void and further related to the generation of inversion domains during the overgrowth [23]. However, in our experiment, no In sub-monolayer or small In clusters are detected in the surrounding matrix, and the missing materials are on the top or top corners of the dots instead of in the middle. Besides, if we treat the 40 nm cap sample as an early stage of the 200 nm cap sample, the In enrichment behaviour from the beginning stage is divergent from that in the GaAs case. In some HAADF images of dots with void, In enrichment is also observed just below the void, challenging the reliability of this material segregation explanation. Nonetheless, the observed stacking faults in the Ge matrix and short line-indentation defects from the AFM images (Figure 4(d) and (e)) should be related to the existence of the nanovoids. The second possibility is related to the heteroepitaxial and capping process strain-induced melting of InAs during overgrowth. For example, the large lattice mismatch-induced heteroepitaxial strain between InAs and GaAs will cause the melting of InAs during the growth on GaAs at 770K [24]. With almost the same lattice constant of Ge

with GaAs, Ge and InAs will also experience quite large heteroepitaxial strain (7.1 %) during the growth. Although the deposition of InAs QD on Ge was carried out at 633 K, the strain caused by the lattice-mismatched heteroepitaxial growth and capping process (at 773 K) might lead to the melting of the dots. Because of higher density of InAs liquid phase than solid phase, the volume of the dots shrinks, and the surrounding Ge, which is stiff to resist a structural change, leads to the formation of void thereafter. During the cooling procedure, in addition, Ge has an even larger TEC than InAs, and thus will shrink faster to its bulk lattice value, locking the location of the nanovoids. This hypothesis can explain the size of the nanovoid and why they did not propagate to the embedment but is unable to clarify the hexagonal shape of the void. The formation of the void facets may involve the varied etching rates of As on InAs along different crystallographic directions during the cooling process, which have been well established in III-V materials [25-27]. Other possibilities of the void formation can be associated with defect-induced deployment of the growing material, but no direct evidence has been found to support all these possibilities.

5. Conclusion

High density InAs QDs have been successfully grown directly on Ge (100) substrates without any buffer layers by solid-source MBE. The overgrowth of Ge was also investigated in detail. In general, the structure of QDs buried in a Ge matrix is more pyramidal and polyhedral, which is different from that in a GaAs or Si matrix and can be mainly attributed to the differences of the TECs of the InAs/Ge and InAs/GaAs systems and suppressed In diffusion from the dots. It was also found that the embedded QD morphology was modified to a large extend during the capping process. While crystal defects, especially SFs and misfit dislocations, are ubiquitous in QDs in both the 40 nm and 200 nm capping layer samples, nanovoids of 7 – 9 nm were presented merely for 200 nm capping layer sample. Possible formation mechanisms are proposed but detailed investigation is demanded in the future. For the 200 nm capped sample, short line indentation planar defects were detected from AFM images, and hints of its formation were also witnessed from STEM images as the propagation of the stacking faults possibly originated from the voids associated with the QDs.

Acknowledgements

This work was supported by UK Engineering and Physical Sciences Research Council (EP/P006973/1, EP/T028475/1), National Epitaxy Facility, European project H2020-ICT-PICTURE (780930) and Royal Academy of Engineering (RF201617/16/28).

References

[1] Chen S *et al* 2016 *Nature Photonics* **10** 307-311
[2] Chen B *et al* 2020 *ACS Photonics* **7** 528-533
[3] Yang J *et al* 2019 *Journal of Crystal Growth* **514** 109-113
[4] Mano T, Fujioka H, Ono K, Watanabe Y and Oshima M 1998 *Applied surface science* **130** 760-764
[5] Cirlin G *et al* 1998 *Semiconductor science and technology* **13** 1262
[6] Hansen L, Bensing F and Waag A 2000 *Thin Solid Films* **367** 85-88
[7] Benyoucef M, Alzoubi T, Reithmaier J, Wu M and Trampert A 2014 *physica status solidi (a)* **211** 817-822
[8] Knuuttila L, Kainu K, Sopanen M and Lipsanen H 2003 *Journal of Materials Science: Materials in Electronics* **14** 349-352
[9] Dhawan T *et al* 2010 *Nanoscale research letters* **5** 31-37
[10] Chaldyshev V, Bert N, Kolesnikova A and Romanov A 2009 *Physical Review B* **79** 233304
[11] Egorov A Y *et al* 1999 *Journal of crystal growth* **201** 1202-1204
[12] Becker R, Klitsner T and Vickers J 1988 *Journal of Microscopy* **152** 157-165
[13] Martin M *et al* 2016 *Applied Physics Letters* **109** 253103
[14] Liu H, Wang T, Jiang Q, Hogg R, Tutu F, Pozzi F and Seeds A 2011 *Nature Photonics* **5** 416-419
[15] Watanabe N, Fukunaga T, Kobayashi K L and Nakashima H 1985 *Japanese journal of applied physics* **24** L498
[16] Bordel D, Guimard D, Rajesh M, Nishioka M, Augendre E, Clavelier L and Arakawa Y 2010 *Applied Physics Letters* **96** 043101
[17] Ledentsov N *et al* 1996 *Physical Review B* **54** 8743
[18] Xie Q, Madhukar A, Chen P and Kobayashi N P 1995 *Physical review letters* **75** 2542
[19] Bert N *et al* 2009 *Semiconductors* **43** 1387-1393
[20] Guffarth F *et al* 2001 *Physical Review B* **64** 085305
[21] Dou W *et al* 2018 *Scientific reports* **8** 1-11
[22] Lenz A *et al* 2004 *Applied physics letters* **85** 3848-3850
[23] Stolyarchuk N, Markurt T, Courville A, March K, Tottereau O, Vennéguès P and Albrecht M 2017 *Journal of Applied Physics* **122** 155303
[24] Bottomley D 1998 *Applied physics letters* **72** 783-785
[25] Huang S, Balakrishnan G, Mehta M, Dawson L, Huffaker D and Li P 2007 *Journal of Applied Physics* **102** 044312
[26] Ibbotson D E, Flamm D L and Donnelly V M 1983 *Journal of applied physics* **54** 5974-5981
[27] Brewer P, McClure D and Osgood Jr R 1985 *Applied physics letters* **47** 310-312